Shape transformation of Pt nanoparticles induced by swift heavy-ion irradiation

R. Giulian,* P. Kluth, L. L. Araujo, and D. J. Sprouster
Department of Electronic Materials Engineering, Research School of Physical Sciences and Engineering, Australian National University, Canberra, Australia ACT 0200

A. P. Byrne
Department of Nuclear Physics, Research School of Physical Sciences and Engineering, Australian National University, Canberra, Australia ACT 0200

D. J. Cookson
Australian Synchrotron Research Program, Argonne, Illinois 60439, USA

M. C. Ridgway
Department of Electronic Materials Engineering, Research School of Physical Sciences and Engineering, Australian National University, Canberra, Australia ACT 0200

(Received 19 June 2008; revised manuscript received 11 August 2008; published 17 September 2008)

Pt nanoparticles (NPs) formed by ion-beam synthesis in amorphous SiO_2 were irradiated with Au ions in the energy range of 27–185 MeV. Small-angle x-ray scattering (SAXS) and transmission electron microscopy were used to characterize an irradiation-induced shape transformation within the NPs. A simple yet effective way of analyzing the SAXS data to determine both NP dimensions is presented. A transformation from spherical to rodlike shape with increasing irradiation fluence was observed for NPs larger than an energy-dependent threshold diameter, which varied from 4.0 to 6.5 nm over 27–185 MeV. NPs smaller than this threshold diameter remained spherical upon irradiation but decreased in size as a result of dissolution. The latter was more pronounced for the smallest particles. The minor dimension of the transformed NPs saturated at an energy-dependent value comparable to the threshold diameter for elongation. The saturated minor dimension was less than the diameter of the irradiation-induced molten track within the matrix. We demonstrate that Pt NPs of diameter 13 nm reach saturation of the minor dimension beyond a total-energy deposition into the matrix of 20 keV/nm^3.

DOI: 10.1103/PhysRevB.78.125413 PACS number(s): 61.80.Jh, 61.46.Hk, 61.72.up, 61.05.cf

I. INTRODUCTION

Nanoparticles (NPs) are promising building blocks for materials with well-defined functions. The understanding of NP properties, which can differ significantly from those of their bulk counterparts, as well as the ability to control parameters such as size, shape, and structure are essential for the development of functional materials and devices.[1] The properties of NPs depend on both size and shape. Examples include linearly polarized emission of semiconductor quantum rods,[2,3] anisotropic magnetic properties of elongated Co NPs,[4] and enhanced catalytic activities of nonspherical Pt NPs.[5]

Ion implantation followed by thermal annealing is a commonly used technique for the fabrication of NPs embedded in a matrix, enabling the control of the depth and concentration of implanted atoms, as well as the protection afforded to the NPs by the surrounding matrix.[6] Ion irradiation prior[7] or subsequent[8,9] to NP formation along with variations in implanted atom concentration and annealing conditions[10] can be used to tailor the size distribution of spherical NPs.

Swift heavy ion irradiation (SHII) is an important tool in the modification of materials.[11–14] In the energy regime above tens of mega electron volts, the ion-matter interaction is dominated by electronic energy loss with the energy locally deposited along the ion path.[15] Effects that arise from this form of interaction include the deformation of metallic and semiconductor NPs. Interestingly, the deformation of semiconductor NPs yields elongation perpendicular to the incident ion-beam direction[16–19] while metallic NPs elongate parallel to the beam direction.[4,20–24] This intriguing behavior of metallic NPs under SHII may yield applications in advanced devices given that NP magnetic[4] and optical[2] properties strongly depend on orientation. D'Orleans *et al.*[4] suggested that NP melting combined with creep deformation drives the elongation process although Klaumunzer[13] pointed out the limitations of such a model. A thorough understanding of the deformation process is still lacking, and only scant and sometimes contradicting results[21,22] have been presented thus far.

This work reports on the effects of SHII of Pt NPs formed by ion implantation in amorphous SiO_2. The deformation process is studied as a function of NP size, irradiation fluence, and energy to give a broad prospective of the shape transformation.

II. EXPERIMENT

Pt NPs were formed in 2-μm-thick SiO_2 films, thermally grown on Si substrates, using ion implantation and thermal annealing. Pt ions of 3.5–5.6 MeV were implanted at liquid N_2 temperature to total fluences of $5\times10^{16}-1\times10^{17}$ cm^{-2}, resulting in peak atomic concentrations of 0.9–3.0 at % at

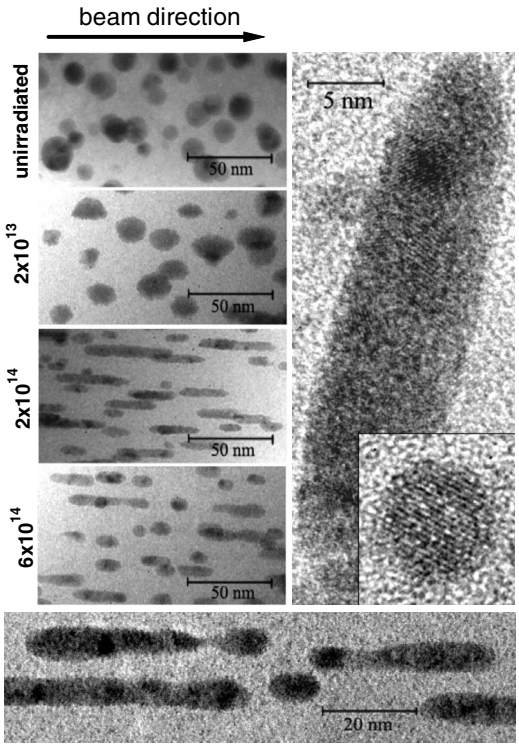

FIG. 1. TEM micrographs of Pt NPs (mean diameter 14.5 nm prior to SHII) irradiated with 185 MeV Au ions at fluences indicated on the panels (left). High resolution images of elongated and spherical Pt NPs (right). Magnified view of Pt NPs irradiated with 4×10^{14} cm^{-2} (bottom).

depths of ~1.4 μm from the SiO_2 surface.[7,10] Samples were subsequently annealed in forming gas ($95\%N_2+5\%H_2$) at different temperatures and different times to generate a variety of NP size distributions. Subsequently, samples were irradiated with 27, 55, 89, or 185 MeV Au ions at room temperature with fluences varying from $1\times10^{12}-2\times10^{15}$ cm^{-2}. The electronic energy loss was near constant over the depth of the SiO_2 layer, and of approximate values of 4, 8, 12, and 17 keV/nm, respectively. The nuclear energy loss was two orders of magnitude lower than the electronic,[25] and was thus considered negligible.

Figure 1 shows transmission electron microscopy (TEM) images of Pt NPs before and after SHII, from which the spherical to rodlike shape transformation is readily apparent. (These micrographs will be further discussed below.) TEM and small-angle x-ray scattering (SAXS) measurements were used to evaluate the shape and size evolution of the Pt NPs. TEM samples were prepared in cross-sectional geometry using the small-angle cleavage technique[26] with the analyses performed with a Philips CM300 microscope operating at 300 kV. SAXS measurements were performed at the ChemMatCARS beamline 15ID-D, Advanced Photon Source, USA, using x rays of wavelength 1.11 Å, and camera lengths of 1880 and 6880 mm. The scattered intensity I was collected as a function of the scattering vector Q using a MAR-165 charge coupled device (CCD) detector with an exposure time of 2 s. The measurements were performed in transmission mode with the sample surface normal oriented at angles of $0°-45°$ relative to the photon beam.

SAXS samples were prepared by our procedure described previously[10] to enable measurements of the NP containing thin films only, avoiding scattering from the Si substrate. First, the Si substrate was thinned to ~150 μm by mechanical grinding. A concavity of 130 μm depth was then formed using a dimple grinder normally utilized for TEM sample preparation. Finally, a hole of diameter ~1 mm was opened in the remaining Si below the SiO_2 layer using selective wet chemical etching in a KOH solution. This method produces self-supporting, thin-film samples ideally suited for transmission SAXS measurements.

III. DATA ANALYSIS

A. Transmission electron microscopy analysis

The NP minor and major dimensions (D_{minor} and D_{major}) were measured directly from TEM images, counting a minimum of 500 particles to achieve reliable statistics. For the comparison of the dimension distributions obtained with SAXS, we estimated the projection of D_{major} (PD_{major}) of the NPs based on the geometry of ellipsoids of revolution

$$PD_{\text{major}} = \sqrt{D_{\text{major}}^2 \sin^2\beta + D_{\text{minor}}^2 \cos^2\beta}, \tag{1}$$

where β is the angle of rotation for the SAXS measurement.

B. Small-angle x-ray scattering analysis

Given the high degree of orientation of the elongated particles as evident in Fig. 1, the distribution of D_{minor} and D_{major} can be obtained from angle-dependent SAXS measurements. This is achieved by the separate analysis of small angular sectors of the detector image to enable the individual evaluation of D_{minor} and PD_{major} of the elongated particles. Figure 2 shows scattering images of samples containing aligned and elongated particles, and schematics of how the x-rays "see" the elongated particles at different angles of rotation. Vertical and horizontal masks of 10° arc sector with origin at the beam stop were used to characterize D_{minor} and PD_{major}, respectively, whose distributions were recovered using the IRENA 2 package for small-angle scattering analysis.[27] Quantitative analysis to determine the NP size distributions was based on a maximum-entropy method[28] using a spherical model.[29] The amplitude for the distribution of the nonspherical particles was corrected after the fit was performed. Since the size distribution of elongated NPs cannot be accurately described as Gaussian or any other common function, we used the maximum-entropy method, which is able to recover distributions of any shape.[28] The use of a spherical particle scattering function in combination with a correction factor substantially simplifies the analysis of highly oriented rods. We established the validity of this approach by comparing SAXS and TEM results, which yielded excellent agreement.

According to the approximate law of Guinier,[29] the scattering intensity $I(Q)$ of nonspherical identical particles can be approximated by

$$I(Q) = n^2 N e^{-Q^2 D^2(l_0)}, \tag{2}$$

where n represents the total number of electrons in each particle, N is the number of particles per unit volume, $D(l_0)$

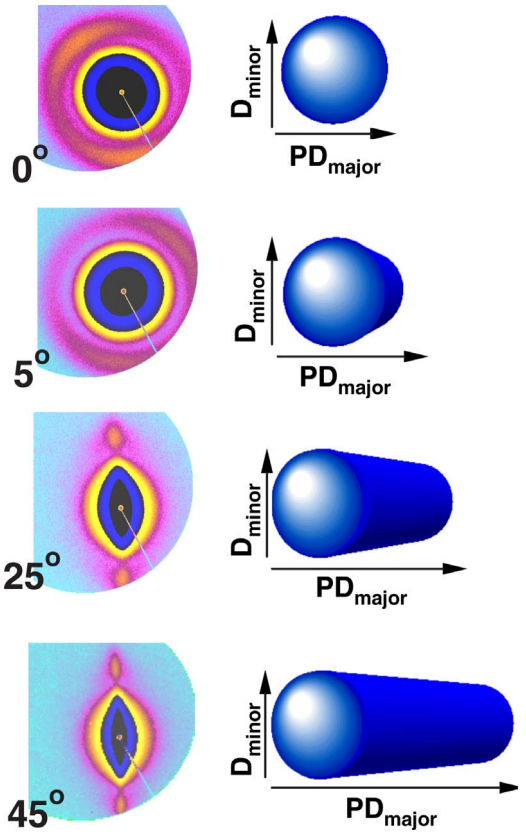

FIG. 2. (Color online) Detector images (left) obtained during the SAXS experiments and schematics of how the x-rays see the elongated particles (right) at different angles of rotation.

is the diameter of the particles in a direction defined by l_0, and Q is the scattering vector defined by

$$Q = 4\pi \frac{\sin\theta}{\lambda}, \tag{3}$$

where 2θ represents the scattering angle and λ the x-ray wavelength. Given that the number of electrons per particle is proportional to the particle volume and using Eq. (1), we related the real volume of the particles and the spherical volume evaluated by the program,

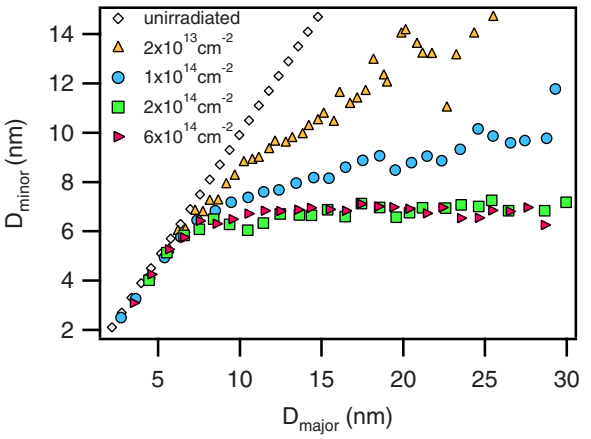

FIG. 3. (Color online) NP D_{major} versus D_{minor} according to SHII fluence, as determined from TEM.

$$V_{\text{real}}^2 N_{\text{real}} = V_s^2 N_s, \tag{4}$$

where V_{real} and N_{real} are the real volume occupied by the particles and the real number of particles, respectively, and V_s and N_S represent the spherical volume and the number of particles estimated by the fitting procedure. From Eq. (4) we defined a correction factor $(V_S^2/V_{\text{real}}^2)$ to be applied to the diameter distributions of nonspherical particles estimated using spherical models.

IV. RESULTS

Figure 1 shows TEM micrographs of Pt NPs irradiated with 185 MeV Au ions. The left panels show the evolution of the NP shape and size as a function of irradiation fluence. Prior to irradiation, the NPs are of diameter 14.5 nm and, as shown in the inset on the right panel of Fig. 1, are spherical and single crystalline. Upon irradiation, the NPs elongate in the direction parallel to the incident ion beam with increasing aspect ratio for fluences $\leq 2\times 10^{14}$ cm^{-2}. They exhibit polycrystalline morphology, as apparent from the high-resolution TEM image shown on the right panel of Fig. 1. For SHII fluences above 2×10^{14} cm^{-2}, the aspect ratio decreases due to dissolution and fragmentation via Rayleigh instability,[30] the latter similar to that observed for annealed nanowires.[31]

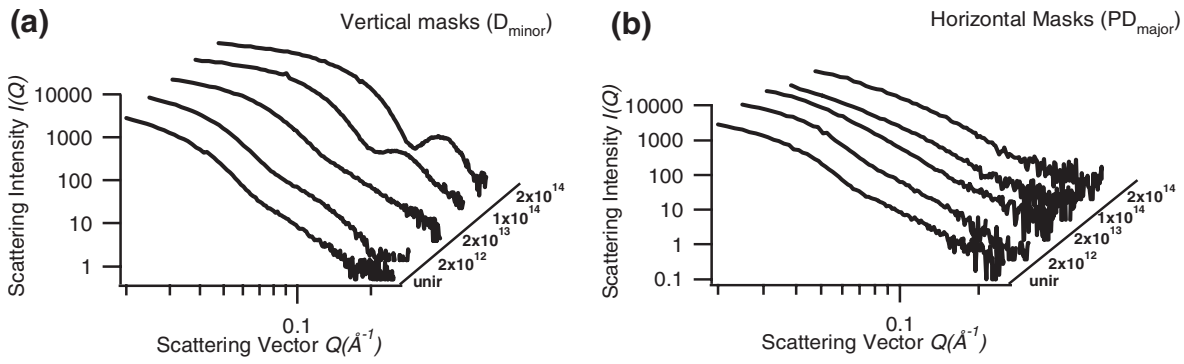

FIG. 4. Scattering intensity $I(Q)$ as a function of the scattering vector Q for Pt NPs with mean diameter 14.5 nm (prior to SHII) irradiated with 185 MeV Au ions at different fluences. Panel (a) shows the scattering integrated from the vertical masks and panel (b) from the horizontal masks, which correspond to the NPs D_{minor} and PD_{major} at 45° sample tilt, respectively.

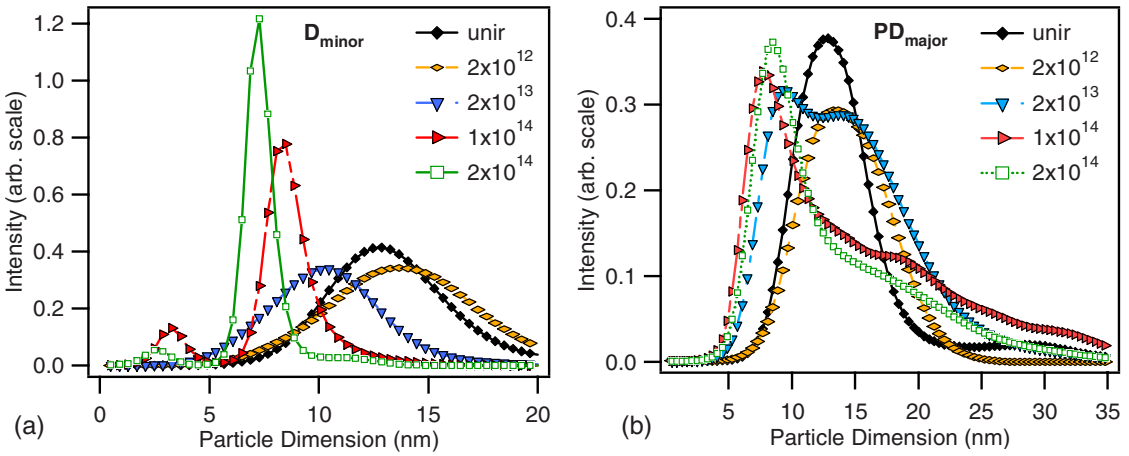

FIG. 5. (Color online) Particle dimension distributions of NPs with mean diameter 14.5 nm (prior to SHII) irradiated with 185 MeV Au at different fluences, as determined from SAXS. Distributions recovered from (a) vertical and (b) horizontal masks corresponding to the NPs D_{minor} and PD_{major}, respectively.

Fragmentation can be observed in the bottom panel of Fig. 1, which shows elongated Pt NPs irradiated with 4×10^{14} cm^{-2}. Surrounding the elongated NPs are very small Pt clusters <1 nm in diameter resulting from NP dissolution. Their small size was below the minimum required for quantitative TEM and SAXS analysis.

The evolution of the NP dimensions under SHII is demonstrated in Fig. 3, which shows D_{minor} as a function of D_{major} measured from TEM micrographs (each point represents the mean value of D_{minor} for a given $D_{\text{major}} \pm 1$ nm). Elongation is only observed for NPs exceeding a threshold diameter of $\sim$6.5 nm for irradiation at 185 MeV. NPs larger than the threshold diameter elongate until D_{minor} saturates at this same threshold value, yielding a very narrow distribution for D_{minor}. Simultaneously, D_{major} increases significantly for SHII fluences $\leq 2 \times 10^{14}$ cm^{-2}, yielding aspect ratios as great as ten (not shown). For higher fluences, despite dissolution and fragmentation, D_{minor} remains unchanged.

Figure 4 shows the complementary scattering intensities as a function of Q following 185 MeV Au ion irradiation. Scattering from the area within the vertical mask is plotted in Fig. 4(a), which originates from D_{minor}, while scattering from the region encompassed by the horizontal mask is plotted in Fig. 4(b), corresponding to PD_{major} at 45°. The corresponding dimension distributions are plotted in Fig. 5, which shows the evolution of D_{minor} and PD_{major} as a function of SHII fluence. The elongation of the NPs upon irradiation broadens the PD_{major} distribution [Fig. 5(b)]. At the same time, the reduction in D_{minor} is accompanied by a narrowing of the D_{minor} distribution [Fig. 5(a)]. The mean dimensions obtained from SAXS analysis of NPs irradiated with 185 MeV Au ions at different fluences, as well as the standard deviation of the distributions (when applicable) and the intensity correction calculated using Eq. (4), are presented in Table I for two NP sizes (8.4 and 14.5 nm prior to SHII). The values listed for the mean dimensions stem from the statistical average of the experimental data, not necessarily coinciding with the peak of the distributions. When the distributions could be approximated by a Gaussian, the standard deviations are also included. Note that for both size distributions,

TABLE I. D_{minor}, PD_{major}, and respective intensity corrections as a function of SHII fluence estimated from SAXS analysis. σ is the standard deviation of the distributions.

		Horizontal Masks			Vertical Masks		
Sample	SHII fluence (cm^{-2})	D_{minor} (nm)	$\sigma_{D_{\text{minor}}}$ (nm)	Intensity correction	PD_{major} (nm)	$\sigma_{PD_{\text{major}}}$ (nm)	Intensity correction
	Unirradiated	8.4	0.9	1	8.5	0.8	1
3 at %	2×10^{12}	7.6	1.3	1	7.7	1.1	1
1200 °C	2×10^{13}	6.8	1.4	0.93	7.0	0.9	1.04
	1×10^{14}	6.5	1.0	0.81	6.9	0.8	1.13
	2×10^{14}	6.4	1.0	0.79	6.8	1.0	1.15
	Unirradiated	14.5	1.8	1	14.4	1.9	1
3 at %	2×10^{12}	14.4	2.3	1	14.3	2.4	1
1300 °C	2×10^{13}	10.9	1.8	0.41	14.4	[a]	2.14
	1×10^{14}	8.8	0.6	0.22	14.7	[a]	4.66
	2×10^{14}	7.3	0.4	0.18	13.1	[a]	6.35

[a]Gaussian approximation not appropriate to fit the distributions.

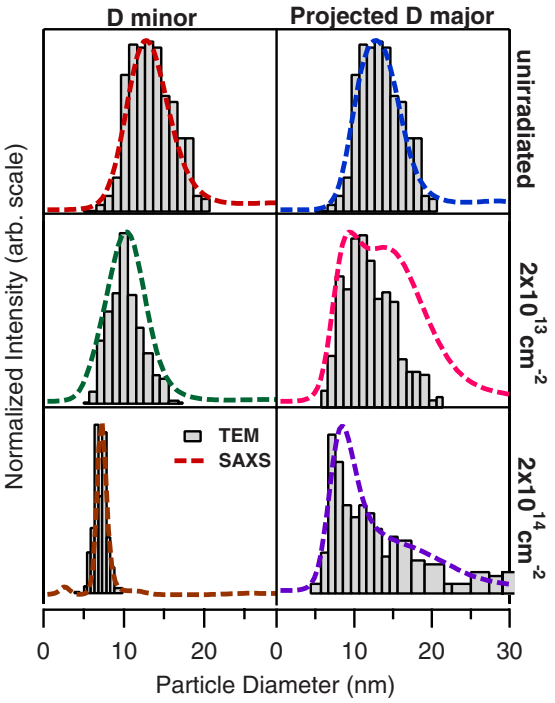

FIG. 6. (Color online) SAXS (lines) and TEM (bars) particle dimension distributions for samples containing NPs with mean diameter 14.5 nm (prior to SHII) irradiated with 185 MeV Au ions at different fluences. The evolution of D_{minor} is displayed on the left while the PD_{major} (at 45° sample tilt) is presented on the right. The TEM distributions for the PD_{major} were geometrically corrected using Eq. (1) to allow the comparison with SAXS results.

the mean NP diameter prior to SHII exceeded the threshold for elongation and, within experimental error, a common saturation value for D_{minor} was observed upon SHII. These results agree well with TEM analysis as shown in Fig. 6, validating our approach used in the SAXS analysis of the rodlike NPs. The TEM distributions were corrected using Eq. (1) to enable comparison with the SAXS results.

Figure 7 shows TEM micrographs of 14.5 nm Pt NPs irradiated with 27, 55, 89, or 185 MeV Au ions to a total fluence of 2×10^{14} cm^{-2}. At this fluence, 89 and 185 MeV irradiations yield a saturation of D_{minor} (as previously demonstrated in Fig. 3 for the latter). However, at lower energies this fluence is insufficient to achieve saturation. 27 MeV/2×10^{14} cm^{-2} irradiation yields images similar to that observed for 185 MeV with a fluence five times lower, where the NPs change from spheres to prolate spheroids. The electronic energy loss is approximately four times greater at 185 MeV compared to 27 MeV. Furthermore, the threshold diameter for elongation decreases with a reduction in ion energy as apparent from Fig. 8, which shows the evolution of D_{major} and D_{minor} following irradiations at different energies. D_{minor} saturation values are approximately 4.3, 5.2, 5.4, and 6.7 nm for 27, 55, 89, and 185 MeV.

Figure 9 shows TEM images of Pt NPs with a mean diameter (3.2 nm) less than the minimum required for elongation. The well-defined NP/matrix interfaces apparent in unirradiated particles [Fig. 9(a)] are lacking following irradiation with 185 MeV Au ions to a total fluence of 3×10^{14} cm^{-2}

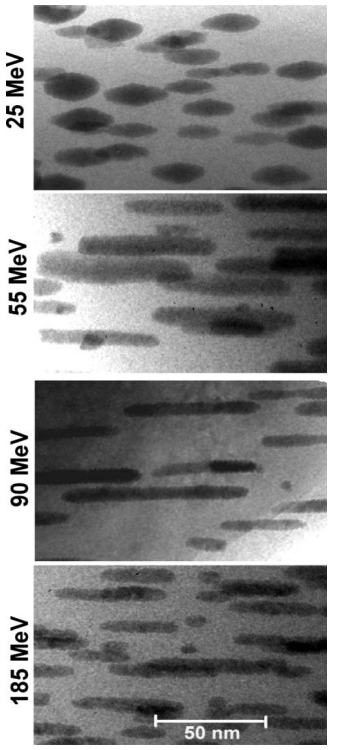

FIG. 7. TEM micrographs of 14.5 nm Pt NPs (prior to SHII) irradiated with 2×10^{14} cm^{-2} at different energies (as shown in each panel).

[Fig. 9(b)]. There is no evidence of a shape change for particles of this size. SHII causes dissolution of the particles, which decrease in size upon irradiation as demonstrated by the SAXS analysis presented in Fig. 10. For NPs of diameter of 3.2 nm irradiated with 185 MeV Au ions, a progressive reduction in NP diameter as a function of increasing irradiation fluence is apparent. The mean NP diameter and the standard deviation of the distributions are presented in Table II as a function of SHII fluence.

From dimension distributions derived from SAXS, we extracted the total volume of scattering particles as a function of SHII fluence and particle size as shown in Fig. 11. (For the SAXS experimental arrangement described herein, we

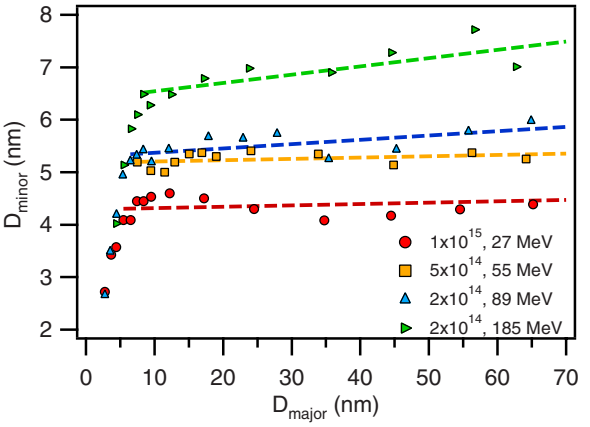

FIG. 8. (Color online) D_{minor} saturation for different energies and fluences (as determined by TEM).

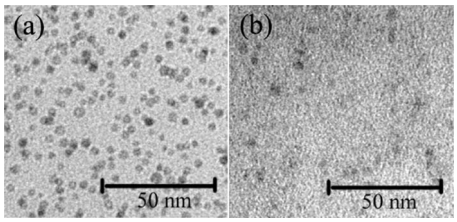

FIG. 9. TEM micrographs of (a) unirradiated Pt NPs with 3.2 nm mean diameter and (b) the same NPs after being irradiated with 185 MeV Au ions to a total fluence of 3×10^{14} cm^{-2}.

are sensitive to NPs of diameter >0.8 nm.) Clearly, smaller NPs are more readily dissolved in the matrix under irradiation, consistent with a larger surface-area-to-volume-ratio.

V. DISCUSSION

The minimum irradiation fluence for which changes in shape were observed was $\sim10^{13}$ cm^{-2}, corresponding to ~15 ion impacts over the cross-sectional area of a NP of diameter 14 nm. Clearly elongation is not a single-ion impact event but it is the result of successive ion/NP/matrix interactions. The shape transformation was observed for all irradiation energies (27–185 MeV) or equivalently over the range of electronic stopping powers (4–17 keV/nm). The latter exceed the threshold (~2 keV/nm) for molten track formation in amorphous SiO_2.[32]

TEM and SAXS results presented here clearly demonstrate that NP volume is not conserved upon irradiation, in contrast to previous reports.[4,18,20,21] Figures 10 and 11 show that the mean diameter and the total volume of NPs contributing to the scattering process decrease as a function of increasing irradiation fluence. Using the mean dimensions derived from SAXS and listed in Table I, the volume of a spherical NP of diameter 14.5 nm is three times that of the rod with minor and major dimensions of 8.8 and 14.7 nm, respectively, observed after 185 MeV Au ion irradiation to a fluence of 1×10^{14} cm^{-2}.

TABLE II. Mean particle diameter (D_{mean}) and standard deviation of the distributions (σ) for each SHII fluence.

Sample	SHII fluence (cm^{-2})	D_{mean} (nm)	σ (nm)
	Unirradiated	3.2	0.4
	1×10^{12}	3.1	0.4
0.9 at %	5×10^{12}	2.9	0.4
1100 °C	1×10^{13}	3.0	0.5
	5×10^{13}	2.7	0.4
	3×10^{14}	2.6	0.3

As demonstrated in Figs. 3 and 8, there is a threshold diameter for NP elongation at each irradiation energy. From a linear fit to the data above this threshold, we extracted the slope that is plotted in Fig. 12 (for NPs of mean diameter 14.5 nm prior to SHII) as a function of the total energy deposited by Au ions in SiO_2. A slope of zero corresponds to the saturation of D_{minor}. Any ion energy dependence is within experimental error. The energy deposition required to reach saturation is necessarily NP size dependent with larger NPs requiring more energy to saturate D_{minor}, as shown in the inset of Fig. 12 for 185 MeV irradiations. The NP volume plotted in the inset is that of the particles before irradiation as estimated from the elongated particle volume corrected to account for dissolution.

As reported by Toulemonde and co-workers,[15,32] SHII of amorphous SiO_2 can result in the formation of a latent track with a diameter dependent on the ion energy. Tracks result from the rapid quenching of a cylinder of matter in which the energy deposited onto the lattice exceeds that necessary for melting. Track diameters range from 6–10 nm for electronic stopping powers of 4–17 keV/nm.[33] Note the similarity between such values, and those for the threshold diameters for elongation and D_{minor} saturations for Pt NPs following SHII. Figure 13 shows theoretical[34] and experimental[35] estimates of the track diameter in SiO_2, and the D_{minor} saturation for Pt NPs as a function of electronic energy loss. The track diam-

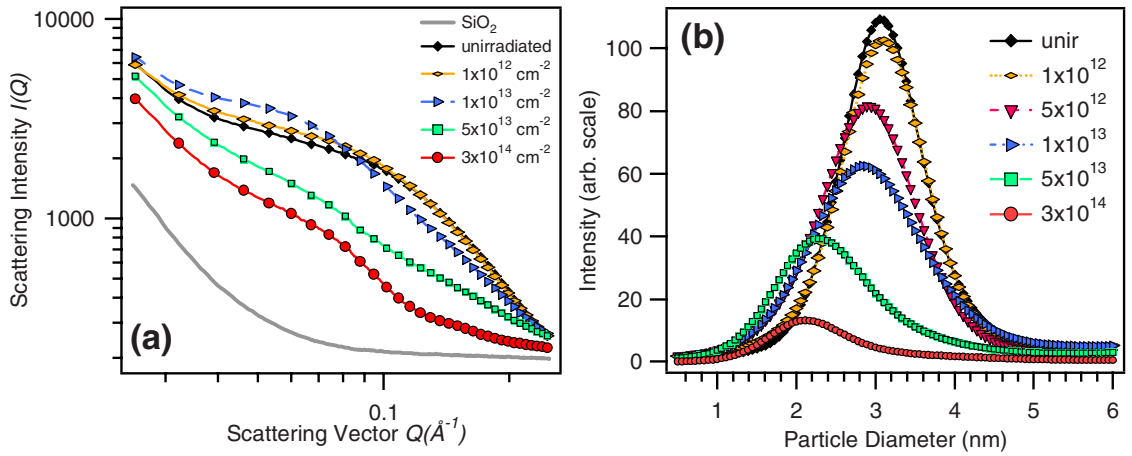

FIG. 10. (Color online) (a) Scattering intensity $I(Q)$ as a function of the scattering vector Q for Pt NPs with mean diameter 3.2 nm (prior to SHII) irradiated with 185 MeV Au ions at different fluences and the scattering contribution of a blank SiO_2; (b) particle diameter distributions for the same samples.

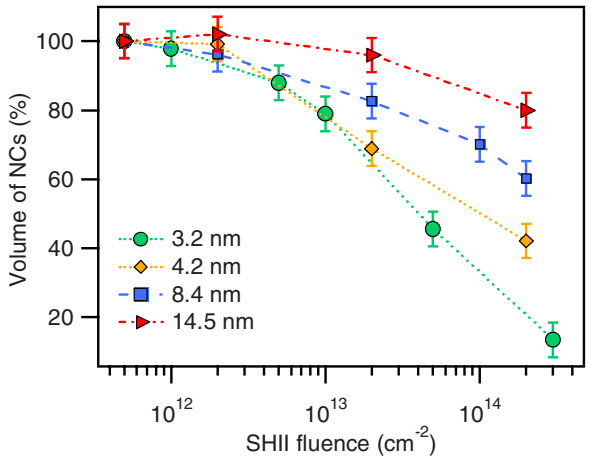

FIG. 11. (Color online) Volume percentage of remaining NPs as a function of SHII fluence. The values are relative to the unirradiated samples and the calculations are based on the total volume occupied by the particles according to SAXS analysis.

eter in SiO_2 is larger than D_{minor} saturation for Pt NPs although both parameters scale with the electronic stopping power. We suggest the elongated metal nanoparticles are confined by the molten track in amorphous SiO_2 and thus the shape transformation will not proceed in the absence of an embedding matrix, consistent with previous observations.[20]

As apparent from Fig. 10(b), Pt NPs below the threshold diameter for elongation dissolve into the matrix upon irradiation. Similar observations were reported by D'Orleans *et al.*[4] for small Co NPs irradiated with 200 MeV *I* ions although the dissolution of small particles was accompanied by the growth of large particles, consistent with Ostwald ripening. The latter was not evident for Pt NPs. Figures 10(b) demonstrated that, respectively, the average particle diameter and the total volume of particles contributing to the scattering process both decreased with irradiation fluence. The dissolved Pt could be in the form of monomers in an oxidized

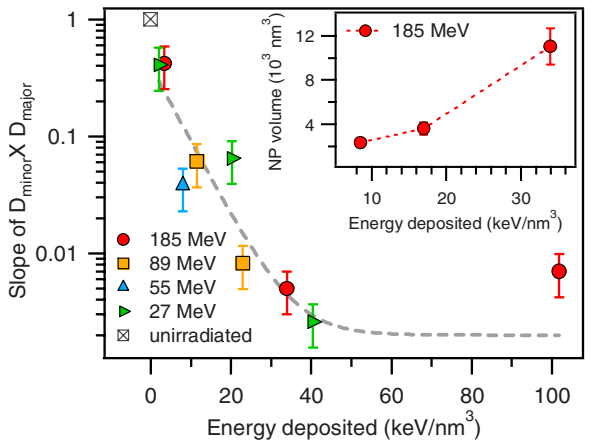

FIG. 12. (Color online) Slope extracted from linear fit to the data above the threshold diameter for elongation presented in Figs. 3 and 8 plotted as a function of energy, deposited for samples containing NPs as large as 19 nm in diameter (prior to SHII). The inset shows the maximum NP volume for D_{minor} saturation as a function of energy deposited (for 185 MeV irradiations).

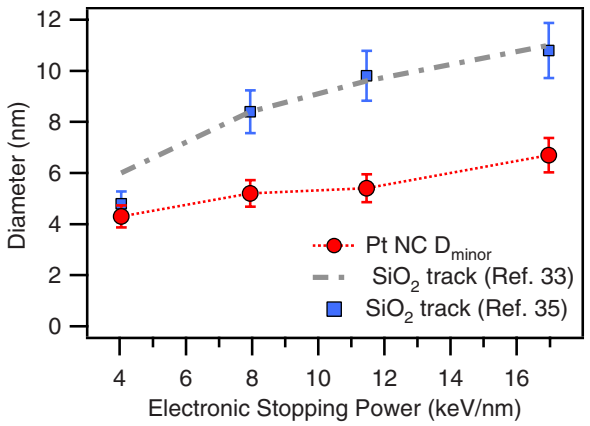

FIG. 13. (Color online) Pt NP D_{minor} (saturation) and SiO_2 track diameter as a function of electronic stopping power. The latter was extracted from Refs. 33 and 35.

environment within the matrix and/or metallic clusters too small (<1 nm) for detection by either TEM or SAXS.

VI. CONCLUSIONS

We have examined the effect of swift heavy ion irradiation on Pt particles embedded in amorphous SiO_2. A shape transformation from spheres to prolate spheroids to elongated rods was observed for NPs exceeding an energy-dependent threshold diameter, where the latter progressively increased as a function of irradiation energy. NPs below this threshold remained spherical but decreased in size until eventually dissolved into the matrix. The dissolution of Pt NPs was size dependent with smaller particles dissolving more rapidly than their larger counterparts. Elongated nanoparticles were also subject to dissolution and, in addition, fragmentation via Rayleigh instability. NPs larger than the threshold diameter were progressively elongated and the minor dimension of the transformed rods saturated at an energy-dependent value that increased as a function of irradiation energy. The total electronic energy deposition necessary to achieve saturation was determined as a function of NP size. As anticipated, larger NPs required greater total-energy deposition to reach saturation. We have correlated the saturation of the minor dimension of elongated particles with the diameter of the molten track in amorphous SiO_2 and suggest that the latter confines the irradiation-induced shape transformation. Such measurements will aid in the identification of the mechanisms governing the elongation process.

ACKNOWLEDGMENTS

We thank the Australian Synchrotron Research Program and the Australian Research Council for financial support. ChemMatCARS Sector 15 at the Advanced Photon Source is principally supported by the National Science Foundation/Department of Energy under Grant No. CHE0087817 and by the Illinois Board of Higher Education. The Advanced Photon Source is supported by the U.S. Department of Energy, Basic Energy Science, Office of Science, under Contract No. W-31-109-Eng-38.

*Corresponding author. raq109@rsphysse.anu.edu.au

[1] E. Roduner, Chem. Soc. Rev. **35**, 583 (2006).
[2] H. Htoon, J. A. Hollingworth, A. V. Malko, R. Dickerson, and V. I. Klimov, Appl. Phys. Lett. **82**, 4776 (2003).
[3] D. Katz, T. Wizansky, O. Millo, E. Rothenberg, T. Mokari, and U. Banin, Phys. Rev. Lett. **89**, 086801 (2002).
[4] C. D'Orleans, J. P. Stoquert, C. Estournes, C. Cerruti, J. J. Grob, J. L. Guille, F. Haas, D. Muller, and M. Richard-Plouet, Phys. Rev. B **67**, 220101 (2003).
[5] R. Narayanan and M. A. El-Sayed, Nano Lett. **4**, 1343 (2004).
[6] A. Meldrum, R. F. Haglund, L. A. Boatner, and C. W. White, Adv. Mater. (Weinheim, Ger.) **13**, 1431 (2001).
[7] R. Giulian, P. Kluth, L. L. Araujo, D. J. Llewellyn, and M. C. Ridgway, Appl. Phys. Lett. **91**, 093115 (2007).
[8] P. Kluth, B. Johannessen, G. J. Foran, D. J. Cookson, S. M. Kluth, and M. C. Ridgway, Phys. Rev. B **74**, 014202 (2006).
[9] B. Johannessen, P. Kluth, R. Giulian, L. L. Araujo, D. J. Llewellyn, G. J. Foran, D. J. Cookson, and M. C. Ridgway, Nucl. Instrum. Methods Phys. Res. B **257**, 37 (2007).
[10] R. Giulian, P. Kluth, B. Johannessen, L. L. Araujo, D. J. Llewellyn, D. J. Cookson, and M. C. Ridgway, Nucl. Instrum. Methods Phys. Res. B **257**, 33 (2007).
[11] S. Klaumunzer and G. Schumacher, Phys. Rev. Lett. **51**, 1987 (1983).
[12] A. Hedler, S. L. Klaumunzer, and W. Wesch, Nat. Mater. **3**, 804 (2004).
[13] S. Klaumunzer, Nucl. Instrum. Methods Phys. Res. B **244**, 1 (2006).
[14] E. Akcoltekin, T. Peters, R. Meyer, A. Duvenbeck, M. Klusmann, I. Monnet, H. Lebius, and M. Schleberger, Nat. Nanotechnol. **2**, 290 (2007).
[15] M. Toulemonde, C. Dufour, and E. Paumier, Acta Phys. Pol. A **109**, 311 (2006).
[16] T. van Dillen, E. van der Giessen, P. R. Onck, and A. Polman, Phys. Rev. B **74**, 132103 (2006).
[17] E. Snoeks, A. van Blaaderen, T. van Dillen, C. M. van Kats, K. Velikov, M. L. Brongersma, and A. Polman, Nucl. Instrum. Methods Phys. Res. B **178**, 62 (2001).
[18] B. Schmidt, A. Mucklich, L. Rontzsch, and K. H. Heinig, Nucl. Instrum. Methods Phys. Res. B **257**, 30 (2007).
[19] S. Klaumunzer, Nucl. Instrum. Methods Phys. Res. B **215**, 345 (2004).
[20] S. Roorda, T. van Dillen, A. Polman, C. Graf, A. van Blaaderen, and B. J. Kooi, Adv. Mater. (Weinheim, Ger.) **16**, 235 (2004).
[21] J. J. Penninkhof, T. van Dillen, S. Roorda, C. Graf, A. van Blaaderen, A. M. Vredenberg, and A. Polman, Nucl. Instrum. Methods Phys. Res. B **242**, 523 (2006).
[22] A. Oliver, J. A. Reyes-Esqueda, J. C. Cheang-Wong, C. E. Roman-Velazquez, A. Crespo-Sosa, L. Rodriguez-Fernandez, J. A. Seman, and N. Cecilia, Phys. Rev. B **74**, 245425 (2006).
[23] P. Kluth, B. Johannessen, R. Giulian, C. S. Schnohr, G. J. Foran, D. J. Cookson, A. P. Byrne, and M. C. Ridgway, Radiat. Eff. Defects Solids **162**, 501 (2007).
[24] B. Joseph, J. Ghatak, H. P. Lenka, P. K. Kuiri, G. Sahu, N. C. Mishra, and D. P. Mahapatra, Nucl. Instrum. Methods Phys. Res. B **256**, 659 (2007).
[25] J. F. Ziegler, J. P. Biersack, and U. Littmark, *The Stopping and Range of Ions in Solids* (Pergamon, New York, 1985).
[26] S. D. Walck and J. P. McCaffrey, Thin Solid Films **308-309**, 399 (1997).
[27] J. Ilavsky, available at http://usaxs.xor.aps.anl.gov/staff/ilavsky/irena.html
[28] J. A. Potton, G. J. Daniell, and B. D. Rainford, J. Appl. Crystallogr. **21**, 891 (1988).
[29] A. Guinier and G. Fournet, *Small-Angle Scattering of X-Rays* (Wiley, New York, 1955).
[30] L. Rayleigh, Proc. London Math. Soc. **s1–10**, 4 (1878).
[31] M. E. Toimil-Molares, A. G. Balogh, T. W. Cornelius, R. Neumann, and C. Trautmann, Appl. Phys. Lett. **85**, 5337 (2004).
[32] M. Toulemonde, C. Trautmann, E. Balanzat, K. Hjort, and A. Weidinger, Nucl. Instrum. Methods Phys. Res. B **216**, 1 (2004).
[33] M. Toulemonde, C. Dufour, E. Paumier, and F. Pawlak, Mater. Res. Soc. Symp. Proc. **504**, 99 (1998).
[34] Z. G. Wang, C. Dufour, E. Paumier, and M. Toulemonde, J. Phys.: Condens. Matter **6**, 6733(1994).
[35] P. Kluth, C. S. Schnohr, O. Pakarinen, F. Djurabekova, D. J. Sprouster, R. Giulian, M. C. Ridgway, A. P. Byrne, D. Trautmann, D. J. Cookson, K. Nordlund, and M. Toulemonde (unpublished).